

Multifunctional Magnetic Bead-Based Dynamic Light Scattering Aptasensor with Rapid and Feasible Determination of Disease-Related Biomarkers

Ying Tang¹, Jin Zhang¹ and Dianping Tang^{2*}

¹Department of Chemistry and Chemical Engineering, Chongqing Key Laboratory of Environmental Materials and Remediation Technologies, Chongqing University of Arts and Sciences, Chongqing, PR China

²Department of Chemistry, MOE Key Laboratory of Analysis and Detection for Food Safety, Fujian Provincial Key Laboratory of Analysis and Detection for Food Safety, Fuzhou University, Fuzhou, PR China

Abstract

A simple and feasible sensing strategy based on target-induced aggregation of aptasensor-conjugated multifunctional magnetic beads was designed for sensitive detection of low-abundant proteins (carcinoembryonic antigen, CEA, used as an example), coupling with dynamic light scattering technique.

Keywords: Aptasensor; Magnetic beads; Dynamic light scattering; Cancer markers

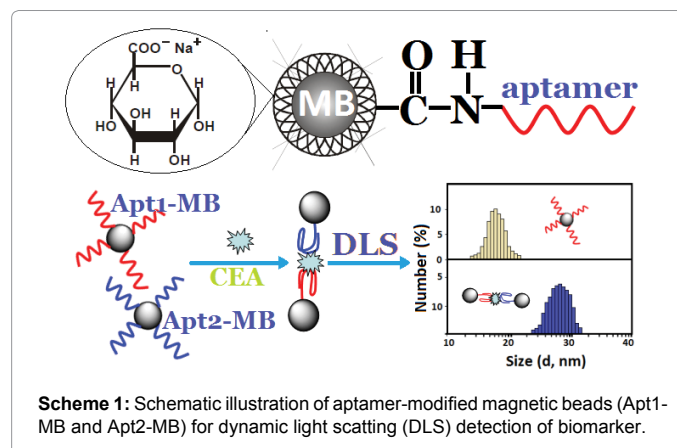
Introduction

Nowadays the existed analytical methods including point-of-care (POC) and the centralized detection in the clinic laboratory have no the ability to meet recent requirements of the patient-friendly testing and increased reliability of results [1,2]. The emerging research field of nanotechnology provides exciting new possibilities for advanced development of new analytical tools [3,4]. Magnetic beads are attractive because they have good biocompatibility and can be separated very readily from the reaction mixtures in an external magnetic field. Magnetic nanoparticles facilitate a wide variety of surface reactions and allow conjugation with biomolecules like proteins and DNA [5,6]. Recent research has looked to develop innovative and powerful novel biofunctionalized magnetic beads, controlled and tailoring their properties in a predictable manner to meet the needs of specific applications [7,8].

Dynamic light scattering (DLS), also known as the photon correlation spectroscopy or quasi-elastic light scattering, is a well-established noninvasive tool for determining the average hydrodynamic diameter (D_H) of particles ranging from 0.5 nm to 10 μ m in suspension or solution [9,10]. Just as unique advantages, DLS-based assays are specifically suitable for nanoparticles-based detection modes [11-13], because they can allow for evaluation of low-concentration levels with the signal amplification and reduce the sample pretreatment requirement in the presence of magnetic particles. Favorably, the biofunctionalized magnetic beads can pull the biomolecules from one laminar flow path to another by applying a local magnetic field gradient and selectively removing them from flowing biological fluids without any washing steps [14,15]. To this end, our motivation in this work is to design magnetic bead-based DLS sensing platform for the detection of disease-related biomarkers by coupling with the aptamer-based sensing system.

Aptamers are single-stranded nucleic acids isolated from random-sequence DNA/RNA libraries by an *in vitro* SELEX [16]. The ability of aptamers to bind to a great variety of targets with high affinity/specificity comparable to that of antibodies makes them promising molecular receptors for bioanalytical applications [17]. Carcinoembryonic antigen (CEA) is recognized as disease-related biomarker to reflect the existence of various cancers and tumors in the human body [18]. So, sensitive

detection of CEA in biological fluids is valuable for clinical diagnosis and treatment assessment of cancers. Herein, we report on the proof-of-concept of a new magnetic bead-based aptasensor for DLS detection of CEA *via* target-induced aggregation of the biofunctionalized nanometer-sized particles (Scheme 1). The sequences of the aptamers for CEA are designed (aptamer-1: 5'-TATCCAGCTTATTCAATT-3'; aptamer-2: 5'-AGGGGG TGAAGGGATACCC-3') [19]. The assay contains two aptamer-functionalized magnetic beads (Apt-MB): aptamer-1-labeled magnetic bead (Apt1-MB) and aptamer-2-labeled magnetic bead (Apt2-MB). In the presence of target CEA, two sets of nanoparticles form a sandwiched complex, which increases with the



Scheme 1: Schematic illustration of aptamer-modified magnetic beads (Apt1-MB and Apt2-MB) for dynamic light scattering (DLS) detection of biomarker.

*Corresponding author: Dianping Tang, Department of Chemistry, MOE Key Laboratory of Analysis and Detection for Food Safety, Fujian Provincial Key Laboratory of Analysis and Detection for Food Safety, Fuzhou University, Fuzhou-350116, PR China, Tel: +059122866125; E-mail: dianping.tang@fzu.edu.cn

Received October 14, 2016; Accepted November 08, 2016; Published November 10, 2016

Citation: Tang Y, Zhang J, Tang D (2016) Multifunctional Magnetic Bead-Based Dynamic Light Scattering Aptasensor with Rapid and Feasible Determination of Disease-Related Biomarkers. J Bioprocess Biotech 6: 287. doi:10.4172/2155-9821.1000287

Copyright: © 2016 Tang Y, et al. This is an open-access article distributed under the terms of the Creative Commons Attribution License, which permits unrestricted use, distribution, and reproduction in any medium, provided the original author and source are credited.

increasing CEA concentration, thus fabricating three-dimensional network with the interleaving bionanoparticles. In this case, the average hydrodynamic diameter D_H increases with the increment of CEA, which can be collected by the photodiode detector and processed through the Malvern Zetasizer nanoapplication software. By monitoring the change in the D_H , we indirectly evaluate the concentration of target CEA in the sample.

Prior to measurement, the aminated aptamers were covalently conjugated to carboxylated magnetic beads (size: 50 nm, 25 mg mL⁻¹, 1.3×10^{16} particles g⁻¹, Chemicell GmbH, Beilin, Germany) *via* typical carbodiimide coupling [20]. Briefly, 110 mg of *N*-hydroxysuccinimide and 15 mg of *N*-(3-dimethylamino propyl)-*N'*-ethyl-carbodiimide hydrochloride were initially added to magnetic suspension (1.0 mL), followed with gentle stirring for 30 min at room temperature. Then, 100 μ L of 100 μ M Apt-1 dissolved into distilled water was injected drop by drop to the suspension under the same conditions. After incubation for 120 min, the conjugates (i.e., Apt1-MB) were magnetically separated, and dispersed in 1.0 mL of 0.01 M PBS, pH 7.4, for further use. By the same token, Apt2-MB was prepared by the same method. Finally, the as-prepared Apt-MB was utilized for the detection of CEA by adding different-concentration standards into the mixture including the equivoluminal Apt1-MB and Apt2-MB (incubation for 60 min at 37°C).

As described above, the change in the D_H derives from the interaction between the conjugated aptamers and target CEA. Thus, the preparation of Apt-MB was very crucial. Figure 1A shows typical transmission electron microscope (TEM; H-7650, Hitachi Instruments, Tokyo, Japan) image of aptamer-conjugated magnetic beads with an average size of ~70 nm, which was almost in accordance with that obtained by DLS data (Figure 1A, inset). Compared with magnetic beads (50 nm), the increasing size was ascribed to the introduction of the aptamers. More significantly, when the as-prepared Apt1-MB and Apt2-MB were incubated with 10 ng mL⁻¹ CEA for 60 min at 37°C, numerous nanoparticles were aggregated together (Figure 1B), and the average size increased to ~450 nm (Figure 1B, inset). Logically, a puzzling question arises to whether the increase in the size derived from the interaction between Apt1-MB and Apt2-MB. To verify this concern, the same-volume Apt1-MB and Apt2-MB were mixed in the absence of target CEA. Experimental results indicated that the average size was almost the same as that in Figure 1A. These results revealed that the increase in the size originated from the specific aptamer-CEA reaction.

Also, we monitored the change in the zeta potential of carboxylated magnetic beads before and after modification with aptamers and target CEA (Apt1-MB used in this case). The zeta potential was -13.7 mV for the carboxylated magnetic beads, which derived from negatively charged carboxyl group. After formation of Apt1-MB, the zeta potential increased to -18.4 mV, which was attributed to negatively charged phosphate backbone of the nucleotides. In contrast, a positive zeta potential (+3.9 mV) was acquired after Apt1-MB reacted with 10 ng mL⁻¹ CEA. The reason might be most likely as a consequence of the fact that the isoelectric point of CEA antigen, as a kind of protein, is less than pH 7.4. In pH 7.4 PBS, CEA antigen is a positively charged species.

Further, fourier transform infrared spectroscopy (FTIR, Vector 22, Bruker) was used for the bioconjugation. It is reported that the shapes of the infrared absorption bands of amide I groups at 1610-1690 cm⁻¹ corresponding to the C=O stretching vibration of peptide linkages and amide II groups around 1500-1600 cm⁻¹ from a combination of

N-H bending and C-N stretching can provide detailed information on the secondary structure of proteins. Figure 2a shows typical FTIR of the carboxylated magnetic beads. An obvious characteristic peak at 1659 cm⁻¹ was observed, which corresponded to the carboxylic group on magnetic beads. When the aminated aptamers were conjugated onto magnetic beads, another characteristic peak at 1543 cm⁻¹ was appeared (Figure 2b), which derived from the N-H bending and C-N stretching. On the basis of the above-mentioned results, we might make a conclusion that the aptamers could be covalently conjugated to magnetic beads by the carbodiimide coupling, and the as-prepared Apt-MB could be used for detection of target CEA.

To further investigate the detectability of the prepared Apt-MB, CEA standards with different concentrations were tested by using DLS on the basis of target-induced aggregation of Apt-MB in 0.01 M PBS, pH 7.4, for incubation 60 min at 37°C. As shown in Figure 3A, the D_H increased with increasing CEA level in the sample. A linear correlation between D_H and CEA level was observed in the dynamic range from 0.5 to 20 ng mL⁻¹ with a detection limit (LOD) of 0.1 ng mL⁻¹ estimated at a signal-to-noise ratio of 3 σ . The LOD of our system was comparable with those of other CEA detection schemes, e.g., hybrid hydrogel photonic barcode-based fluorescent assay (0.78 ng mL⁻¹) [21], carbon dots-based fluoremetric detection (0.3 ng mL⁻¹) [22], 3-D surface molecular imprinting-based electrochemical readout (0.5 ng mL⁻¹) [23], quantum dot-based microarray immunoassay (0.19 ng mL⁻¹) [24], and impedimetric immunosensor (1.0 ng mL⁻¹) [25]. Due to the threshold value of CEA (3.0 ng mL⁻¹) in normal human serum, our method could completely meet the needs of CEA detection.

To investigate the reproducibility of determinations, we repeatedly assayed 4 different concentrations of analyte, using identical batches of Apt1-MB and Apt2-MB. Experimental results indicated that the

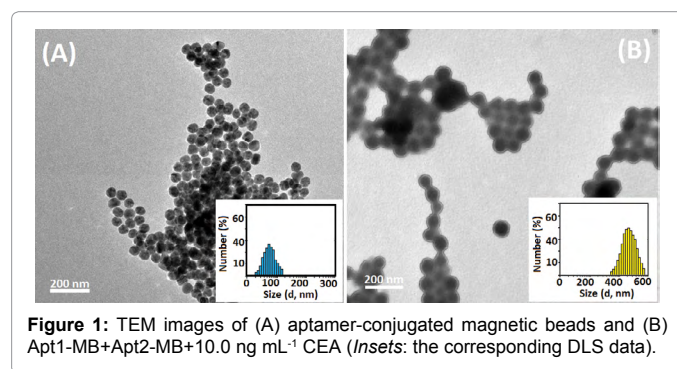


Figure 1: TEM images of (A) aptamer-conjugated magnetic beads and (B) Apt1-MB+Apt2-MB+10.0 ng mL⁻¹ CEA (Insets: the corresponding DLS data).

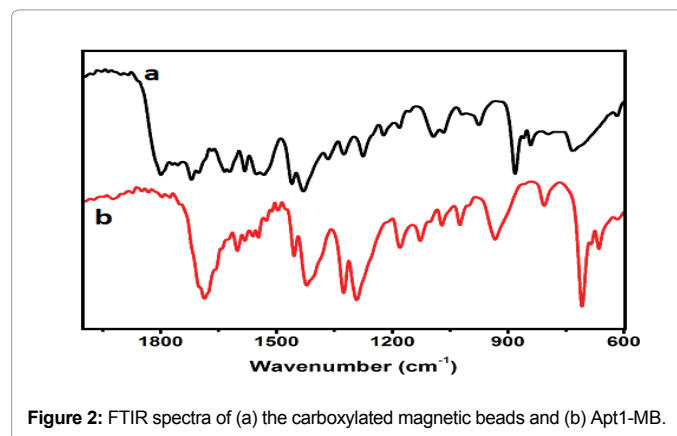


Figure 2: FTIR spectra of (a) the carboxylated magnetic beads and (b) Apt1-MB.

coefficients of variation (CVs) of the intra-assay between five runs were 9.1%, 7.3%, 6.2%, and 8.6% for 0.5 ng mL⁻¹, 1.0 ng mL⁻¹, 5.0 ng mL⁻¹, and 15 ng mL⁻¹ CEA, respectively, whereas the CVs of the inter-assay with various batches were 13.2%, 9.7%, 8.5%, and 10.6% towards the above mentioned analyte. With the exception of the slightly increased CV for the 0.5 ng mL⁻¹ standard in the inter-assay experiment, the other CVs indicated that the aptasensor could be used repeatedly, and further verified the possibility of batch preparation. When the Apt1-MB and Apt2-MB were not in use, they were stored at 4°C. No obvious change was observed after storage for 30 days but an 8.9% decrease of its initial signal was noticed after 90 days.

Next, the specificity of DLS-based aptasensor was studied by assaying other biomarkers, e.g., cancer antigen 19-9 (CA 19-9), alpha-fetoprotein (AFP), cancer antigen 125 (CA 125) and prostate specific antigen (PSA). As shown in Figure 3B, the D_H of aptasensor toward non-target analytes was almost the same as the background signal. High D_H could be only achieved toward target CEA. Significantly, the presence of non-target analytes did not obviously affect the D_H change of the aptasensor. These results revealed that our strategy had good reproducibility and precision, high selectivity and long-term stability.

To further investigate the accuracy of our method, 13 human serum specimens containing different-concentration CEA sample, gifted from Southwest Hospital (Chongqing, China) according to the rules of the local ethical committee, were monitored by using the aptasensor and commercial CEA ELISA kit (Sigma-Aldrich). Prior to measurement, these samples were gently shaken at room temperature (Note: all handling and processing were performed carefully, and all tools in contact with patient specimens and immunoreagents were disinfected after use), and then evaluated by using these two methods. The data obtained by two methods were fitted with a regression equation $y=0.9536x+1.1648$ ($R^2=0.9884$, $n=13$), indicating a highly positive correlation between two methods (Figure 4). Thus, the DLS-based aptasensor could be used for quantitative monitoring of target CEA in the complex samples.

In summary, this work reports on the proof-of-concept of a simple and powerful aptasensing system with the dynamic light scattering based on aptamer-functionalized magnetic beads. Sandwich-type assay format was used for quantitative monitoring of disease-related biomarker. Experimental results revealed that the D_H change of the aptasensor was very strong before and after the reaction of aptamer

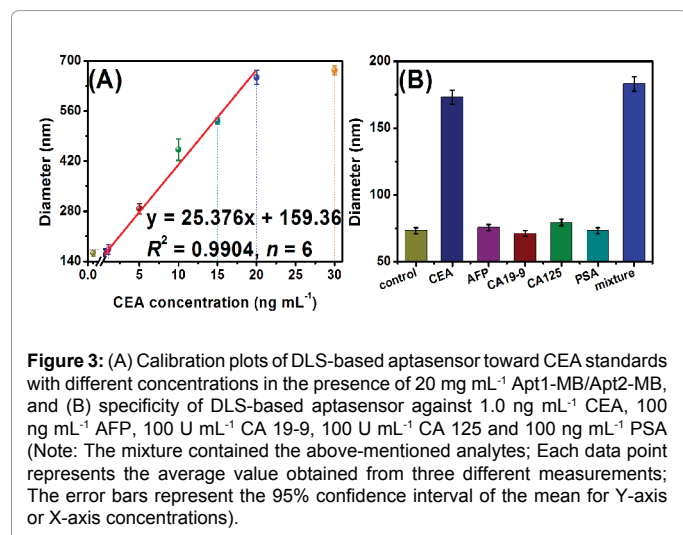


Figure 3: (A) Calibration plots of DLS-based aptasensor toward CEA standards with different concentrations in the presence of 20 mg mL⁻¹ Apt1-MB/Apt2-MB, and (B) specificity of DLS-based aptasensor against 1.0 ng mL⁻¹ CEA, 100 ng mL⁻¹ AFP, 100 U mL⁻¹ CA 19-9, 100 U mL⁻¹ CA 125 and 100 ng mL⁻¹ PSA (Note: The mixture contained the above-mentioned analytes; Each data point represents the average value obtained from three different measurements; The error bars represent the 95% confidence interval of the mean for Y-axis or X-axis concentrations).

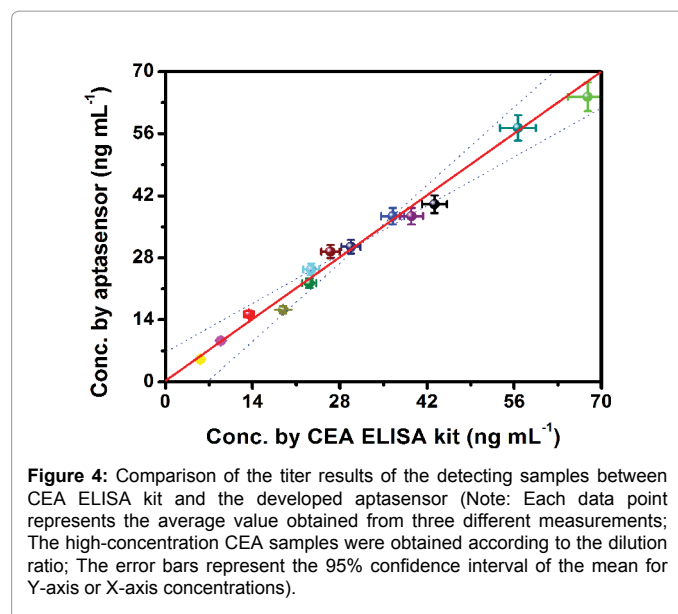


Figure 4: Comparison of the titer results of the detecting samples between CEA ELISA kit and the developed aptasensor (Note: Each data point represents the average value obtained from three different measurements; The high-concentration CEA samples were obtained according to the dilution ratio; The error bars represent the 95% confidence interval of the mean for Y-axis or X-axis concentrations).

with target analyte. Highlight of this work is to exploit a new type of nanoparticle-based DLS aptasensor for the amplification of the detectable signal. These features, as well as its other advantages, such as operation convenience, enzyme-free, and low cost, make it further applicable for other proteins or biomolecules by controlling target antibody, thus demonstrating the versatility of the proposed assay.

Acknowledgements

This work was supported by the National Natural Science Foundation of China (21675029, 21475025), Doctoral Program of Higher Education of China (20134103120002), the Chongqing Science and Technology Commission, China (CSTC2015JCYJB X0126, CSTC2016SHMSZX20001) and the Scientific Research Foundation from Chongqing University of Arts and Sciences (R2013CJ03).

References

- Chen S, Wan Q, Badu-Tawiah AK (2016) Mass Spectrometry for Paper-based Immunoassays: Towards On-demand Diagnosis. *J Am Chem Soc* 138: 6356-6359.
- Frueh FW, Greely HT, Green RC, Hogarth S, Siegel S (2011) The future of direct-to-consumer clinical genetic tests. *Nat Rev Gen* 12: 511-515.
- Pei X, Zhang B, Tang J, Liu B, Lai W, Tang D (2013) Sandwich-type immunosensors and immunoassays exploiting nanostructure labels: A review. *Anal Chim Acta* 758: 1-18.
- Tang D, Cui Y, Chen G (2013) Nanoparticle-based immunoassays in the biomedical field. *Analyst* 138: 981-990.
- Tang D, Su B, Tang J, Ren J, Chen G (2010) Nanoparticle-based sandwich electrochemical immunoassay for carbohydrate antigen 125 with signal enhancement using enzyme-coated nanometer-sized enzyme-doped silica beads. *Anal chem* 82: 1527-1534.
- Zhang B, Liu B, Tang D, Niessner R, Chen G, et al. (2012) DNA-Based Hybridization Chain Reaction for Amplified Bioelectronic Signal and Ultrasensitive Detection of Proteins. *Anal. Chem* 84: 5392-5399.
- Gao Z, Xu M, Hou L, Chen G, Tang D (2013) Magnetic Bead-Based Reverse Colorimetric Immunoassay Strategy for Sensing Biomolecules. *Anal Chem* 85: 6945-6952.
- Tang D, Liu B, Niessner R, Li P, Knopp D (2013) Target-Induced Displacement Reaction Accompanying Cargo Release from Magnetic Mesoporous Silica Nanocontainers for Fluorescence Immunoassay. *Anal Chem* 85: 10589-10596.
- Roger V, Cottet H, Cipelletti L (2016) A New Robust Estimator of Polydispersity from Dynamic Light Scattering Data. *Anal Chem* 88: 2630-2636.

10. Cheng K, Lee P, Qasim M, Liu C, Cheng W, et al. (2016) Electrically Switchable and Permanently Stable Light Scattering Modes by Dynamic Fingerprint Chiral Textures. *ACS Appl Mater Interfaces* 8: 10483-10493.
11. Zheng T, Cherubin P, Cilenti L, Teter K, Huo Q (2016) A simple and fast method to study the hydrodynamic size difference of protein disulfide isomerase in oxidized and reduced form using gold nanoparticles and dynamic light scattering. *Analyst* 141: 934-938.
12. Li C, Ma J, Fan Q, Tao Y, Li G (2016) Dynamic light scattering (DLS)-based immunoassay for ultra-sensitive detection of tumor marker protein. *Chem Commun* 52: 7850-7853.
13. Fu C, Ma H, Huang C, Jia N (2015) A simple and dual functional dynamic light scattering (DLS) probe for rapid detection of mercury ions and biothiols. *Anal Methods* 7: 7455-7460.
14. Zhang Y, Xue Q, Liu J, Wang H (2017) Magnetic bead-liposome hybrids enable sensitive and portable detection of DNA methyltransferase activity using personal glucose meter. *Biosens Bioelectron* 87: 537-544.
15. Decrop D, Brans T, Gijssbergh P, Lu J, Spasic D, et al. (2016) Optical Manipulation of Single Magnetic Beads in a Microwell Array on a Digital Microfluidic Chip. *Anal Chem* 88: 8596-8603.
16. Perez-Ruiz E, Lammertyn J, Spasic D (2016) Evaluation of different strategies for magnetic particle functionalization with DNA aptamers. *New Biotechnol* 33: 755-762.
17. Citartan M, Chng E, Rozhdestvensky R, Tang T (2016) Aptamers as the 'capturing' agents in aptamer-based capture assays. *Microchem J* 128: 187-197.
18. Jin Y, Mao H, Jin Q, Zhao J (2016) Real-time determination of carcinoembryonic antigen by using a contactless electrochemical immunosensor. *Anal Methods* 8: 4861-4866.
19. Wang D, Li Y, Lin Z, Qiu B, Guo G (2015) Surface-Enhanced Electrochemiluminescence of Ru@SiO₂ for Ultrasensitive Detection of Carcinoembryonic Antigen. *Anal Chem* 87: 5966-5972.
20. Kandimalla V, Tripathi V, Ju H (2006) A conductive ormosil encapsulated with ferrocene conjugate and multiwall carbon nanotubes for biosensing application. *Biomaterials* 27: 1167-11174.
21. Xu Y, Zhang X, Luan C, Wang H, Chen B, et al. (2017) Hybrid hydrogel photonic barcodes for multiplex detection of tumor markers. *Biosens Bioelectron* 87: 264-270.
22. Miao H, Wang L, Zhuo Y, Zhou Z, Yang X (2016) Label-free fluorimetric detection of CEA using carbon dots derived from tomato juice. *Biosens Bioelectron* 86: 83-89.
23. Yu Y, Zhang Q, Buscaglia J, Chang C, Liu Y, et al. (2016) Quantitative real-time detection of carcinoembryonic antigen (CEA) from pancreatic cyst fluid using 3-D surface molecular imprinting. *Analyst* 141: 4424-4431.
24. Liu L, Wu S, Jing F, Zhou H, Jia C, et al. (2016) Bead-based microarray immunoassay for lung cancer biomarkers using quantum dots as labels. *Biosens Bioelectron* 80: 300-306.
25. Yeh C, Su K, Lin Y (2016) Development of an impedimetric immunobiosensor for measurement of carcinoembryonic antigen. *Sens Actu A* 241: 203-211.